*engineering proceedings*

MDPI

*Proceeding Paper*

# Time-Dependent Modeling of an Electrochemical Impedance Spectroscopy-Based Sensor †

**Yawar Abbas *, Laura van Smeden, Alwin R. M. Verschueren, Marcel A. G. Zevenbergen and Jos F. M. Oudenhoven**

imec at Holst Centre, 5656 AE Eindhoven, The Netherlands; email1@email.com (L.v.S.); email2@email.com (A.R.M.V.); email3@email.com (M.A.G.Z.); email4@email.com (J.F.M.O.)

* Correspondence: yawar.abbas@imec.nl

† Presented at The 11th International Electronic Conference on Sensors and Applications (ECSA-11), 26–28 November 2024; Available online: https://sciforum.net/event/ecsa-11.

**Abstract:** A time-dependent electrochemical impedance spectroscopy (EIS) model is presented, using a finite element method (FEM) for a 2D interdigitated electrode in an aqueous NaCl electrolyte. Developed in COMSOL Multiphysics, the model incorporates ion transport, potential drop, electric field, Stern layer, and electrode sheet resistance. The current response shows a time-dependent behavior as it needs some periods to stabilize, giving an important insight into determining the number of excitation periods before evaluating the impedance. Three different NaCl electrolyte concentrations are simulated and compared with the experimental data. The simulation results reproduce the characteristic features of the measurements, albeit not quantitatively accurate.

**Keywords:** electrochemical impedance spectroscopy; simulation; COMSOL model; experimental validation

**Citation:** Abbas, Y.; van Smeden, L.; Verschueren, A.R.M.; Zevenbergen, M.A.G.; Oudenhoven, J.F.M. Time-Dependent Modeling of an Electrochemical Impedance Spectroscopy-Based Sensor. *Eng. Proc.* **2024**, *5*, x. https://doi.org/10.3390/xxxxx

Academic Editor(s): Name

Published: 26 November 2024



## 1. Introduction

Electrical impedance spectroscopy (EIS) is a widely used technique in electrochemical sensing [1,2]. As a non-invasive and (often) label-free method, EIS facilitates the analysis of biological samples exposed to an oscillating electric field between working and counter electrodes [3]. This technique is fundamental in investigating the properties of electrode surfaces and bulk electrolytes in various electrochemical sensors [4]. EIS spans a broad frequency range, providing different insights at different frequencies. At low frequencies (typically below 100 Hz), the technique is particularly adept at probing the electrode-electrolyte interface, revealing critical information about the double-layer capacitance [2,4]. In contrast, at higher frequencies (typically above 1 kHz), the influence of the double-layer capacitance wanes, and the impedance response is primarily dictated by the resistance of the electrolyte [4–6].

The design of efficient EIS electrodes necessitates a profound understanding of both the electrode-electrolyte interface and the bulk electrolyte properties, ensuring optimal sensor performance. The finite element method has become an important tool for modelling electrochemical systems [7]. These simulations enable the exploration of various design and parametric configurations, providing an assessment of system behavior and outcomes under different conditions, such as geometries, surface morphologies, material properties, and testing environments. COMSOL Multiphysics® is tool to make a finite element model, supporting Multiphysics simulations of complex geometries and integrating a wide range of physical phenomena, including hydrodynamic and electrochemical processes. Simplified models are frequently used, like the Randles equivalent circuit [8], with electric double layer (EDL) capacitance $C_{dl}$ and electrolyte resistance $R_s$ in series. The charge transfer resistance element $R_{ct}$ is often disregarded when modeling EIS based

sensors, since the electrodes are ideally polarizable. Randles circuits offer basic estimations but prove inadequate for complex geometries such as planar interdigitated electrodes and electrolytes undergoing bulk reactions. Moreover, non-linear time dependent behavior cannot be evaluated from the Randles circuit. Whereas FEM-based model can cover the complex geometric aspect as well as can perform time-dependent non-linear analysis. Analytical models typically offer steady-state analysis, whereas time-dependent numerical models delve deeper, offering comprehensive insights into the dynamic processes occurring at the electrode-electrolyte interface during electrode excitation.

Several efforts to model EIS-based sensors have been reported in the literature, spanning applications such as fuel cells, biosensing, and environmental sensing [9,10]. In most of the reported models, a stationary study is considered with the whole system in the steady state. On the other hand, some studies have implemented time-dependent analyses, primarily for fuel cells using porous mixed ionic-electrolyte conducting (MIEC) cathode materials for gas reduction reactions [10]. For fuel cells, time-dependent analysis of impedance is crucial for understanding the effects of various rate-limiting steps. These studies highlight the advantage of analyzing the transient response of current over time, emphasizing the waiting period until the current response reaches a steady state. However, for sensing applications using a polarizable electrode in an aqueous electrolyte—where the flux is generated by ion transport over time—such analyses have to our knowledge not been reported. Insights into the transient response of surface phenomena at the electrode-electrolyte interface, including the Stern and Debye layers, need to be explored.

In this study, we present the development of a COMSOL-based time-dependent model aimed at stimulating the EIS response of a planar interdigitated electrode (two-electrode) sensor. The model will compute the ion transport resulting from an applied excitation voltage. For simplicity, a monovalent salt solution, such as NaCl electrolyte, with various concentration is used for model validation. The Stern layer voltage-drop, sheet resistance of the electrode and the development of the Debye layer is investigated. To validate the model, lab experiments, with an interdigitated electrode are performed, and the EIS plots from the experimental data are compared with the simulations. Currently, the model has been validated using bare platinum electrodes, and future work will involve functionalizing these electrodes with bioreceptors to enhance selectivity.

## 2. Material and Methods

### *2.1. EIS Measurement*

Electrochemical Impedance Spectroscopy (EIS) operates by perturbing an electrochemical system with a sinusoidal signal, such as an AC excitation potential, across a wide frequency spectrum. The system's corresponding sinusoidal response, in the form of current, is then measured and analyzed in response to this applied perturbation. Typically, a sinusoidal voltage excitation signal, $\varphi_{(t)}$, (Equation (1)) with an amplitude, $\varphi_0$, and angular frequency, $\omega$, is applied between two electrodes and the current response is measured. The current response, $I_{(t)}$, is also a sinusoidal response, with angular frequency, $\omega$, and a phase shift, $\phi$ (Equation (2)). The resulting impedance, Z, can be defined by the magnitude of impedance, $|Z|$, and the phase shift. By Ohm's law the magnitude of impedance is given by the Voltage amplitude divided by the current response amplitude and the phase shift by the phase difference between the voltage and current response peak, i.e., $|Z| = \varphi_0/I_0$, from Equations (1) and (2).

$$\varphi_{(t)} = \varphi_0 Sin(\omega t) \quad (1)$$

$$I_{(t)} = I_0 Sin(\omega t + \phi) \quad (2)$$

In this study, an interdigitated platinum electrode pair on a silicon substrate with an $SiO_2$ isolation layer is used for the validation of the COMSOL model, shown as a schematic

in Figure 1. This modeling must account for the parasitic effects of the $SiO_2$ layer (500 nm thick), which introduces an additional parasitic capacitance, $C_{par}$. Moreover, the sheet resistance of the planar electrode, $R_{el}$, is also considered in this model.

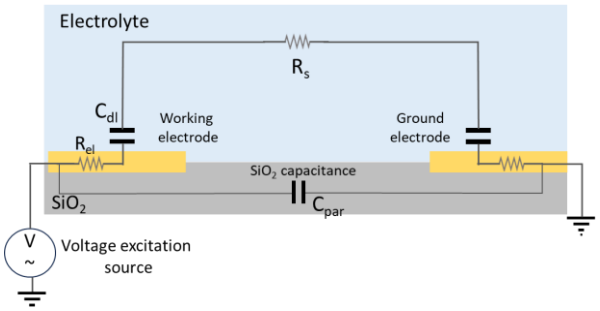


**Figure 1.** Schematic of the equivalent component and elements for the sensor used in this study.

*2.2. COMSOL Model Details*

The COMSOL model is built as a two-dimensional model to compute the voltage drop and the ion concentrations in the electrolyte. The model definition for the planar interdigitated electrode is shown in Figure 2. To solve the voltage and the ion concentrations in the domain, two equations are used: Poisson and Nernst-Planck. The details of the all the symbols in Figure 2 are given in Table 1.

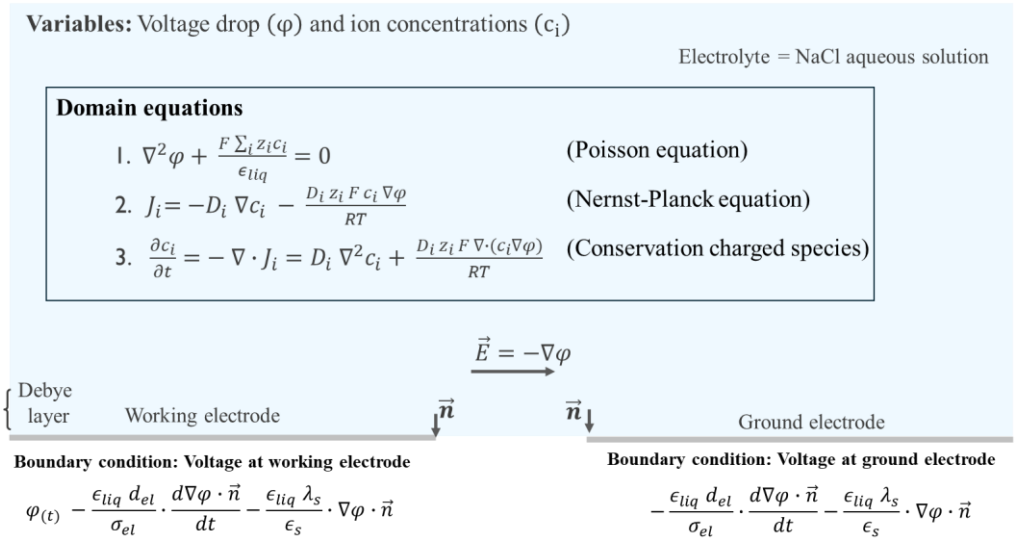


**Figure 2.** Model definition of the time dependent based modeling for electrochemical impedance spectroscopy.

The Stern layer, which forms the innermost region of the electrical double layer (EDL), typically consists of ions that are oppositely charged to the surface and are electrostatically bound to it. These adsorbed ions within or adjacent to the Stern layer exhibit no relative motion with respect to the surface due to the strong adsorption forces. In contrast, ions within the diffuse layer exhibit greater mobility, as they are not as strongly bound to the surface. Moreover, due to the sheet resistance of the electrode, a resistive element at the electrode surface is also included. These inclusions constitute the boundary conditions at the electrode. At the working electrode boundary, the potential is equal to the excitation voltage minus the voltage drop due to the sheet resistance ($\frac{d_{el}}{\sigma_{el}}$) and Stern layer thickness ($\lambda_S$), as shown in Figure 2. Whereas at the ground electrode boundary the potential is equal to the voltage drop due to sheet resistance and Stern layer. These two terms, $\frac{\epsilon_{liq} d_{el}}{\sigma_{el}}$

and $\frac{\epsilon_{liq} \cdot \lambda_S}{\epsilon_S}$ are denoted as $k_{el}$ and $k_s$, respectively and are used as parameters and their values are determined by fitting the simulations to the experiments, and afterwards checked for physical plausibility. Both parameters have different S.I units, as given in Table 2. The Stern layer is modeled as a dielectric layer with a defined thickness and constant permittivity, analogous to a capacitor, where the potential drop is determined by the variation of the electric field at the electrode surface. This approach is also consistent with surface charge-based model.

**Table 1.** Overview of used symbols and their definitions.

| Symbol | Details |
|---|---|
| $c_i$ | Concentration of ion species i [mol/m$^3$] |
| $D_i$ | Diffusion coefficient of species i [m$^2$/s] |
| $z_i$ | Charge number of ion species i |
| $\lambda_s$ | Stern layer thickness [m] |
| $\epsilon_s$ | Stern layer permittivity [F/m] |
| $\epsilon_{liq}$ | Electrolyte permittivity [F/m] |
| $\sigma_{el}$ | Conductivity of the electrode material [S/m] |
| $d_{el}$ | Electrode thickness [m] |
| $\varphi$ | Potential in the electrolyte [V] |
| $\varphi_{y=0}$ | Potential at the working electrode [V] |
| $\varphi_{y=L}$ | Potential at the ground electrode [V] |
| $\varphi_{(t)}$ | Applied external voltage at the working electrode [V] |
| $\vec{n}$ | Normal unit vector to surface |
| $J_i$ | Flux of ion species i [mol/(m$^2$ s)] |
| $\vec{E}$ | Electric field [V/m] |

2.2.1. Parameters

The parameters and initial conditions of the system must be defined at the start, as detailed in Table 2. These parameters are used in the domain equations and boundary conditions. Three different salt concentrations—1 mM, 10 mM, and 100 mM—are used to examine the effect of bulk ion concentration. For the sinusoidal voltage excitation, an amplitude of 10 mV with a frequency sweep from 0.1 Hz to 1 MHz is applied.

**Table 2.** Parameters and its values in the model.

| Symbol | Details |
|---|---|
| $c_{bulk}$ | Bulk concentration of $Na^+$ and $Cl^-$ ions, respectively, 1 mM, 10 mM and 100 mM |
| $D_{Na}$ | Diffusion coefficient of $Na^+$, $1.33 \cdot 10^{-9}$ m$^2$/s [11] |
| $D_{Cl}$ | Diffusion coefficient of $Cl^-$, $2.03 \cdot 10^{-9}$ m$^2$/s [11] |
| $z_i$ | +1 for $Na^+$ ion and −1 for $Cl^-$ ion |
| $\lambda_s$ | 0.5 nm [12] |
| $\epsilon_{liq}$ | Relative permittivity of the electrolyte, 80 |
| $\varphi_{(t)}$ | 10 mV amplitude sinusoidal excitation voltage |
| $f$ | Excitation frequency (0.1 Hz to 1 MHz) |
| $k_{el}$ | Electrode sheet resistance parameter. varied range in simulations: $1 \cdot 10^{-13}$ to $1 \cdot 10^{-11}$ m·s |
| $k_s$ | Stern layer parameter: varied range in simulations $1 \cdot 10^{-11}$ to $1 \cdot 10^{-10}$ m |
| $C_{par}$ | Parasitic capacitance from $SiO_2$ layer: 0.7 nF |

2.2.2. Model Geometry

The design of the Interdigitated Electrodes (IDEs) used for model validation is shown in Figure 3a. Modeling such a geometry and dimension in 3D requires significantly more computational time and resources. Therefore, a 2D approximation of the IDE design is employed. This 2D approximation is done by considering the cross-section of the half of

the electrode width of first electrode finger set at one end of the IDEs and then unfolding the meander spacing between the IDEs. The IDEs is approximated as two parallel planar electrodes with electrode spacing, S, and electrode width, W/2 (half of the width of one electrode finger) and length equal to the total length of the meander spacing, $L_m$. A two parallel planar electrode can be modeled in 2D, as shown in Figure 3b, where the electrode length, $L_m$, is added later for scaling the current response values. The values of all the model dimensions are given in Table 3.

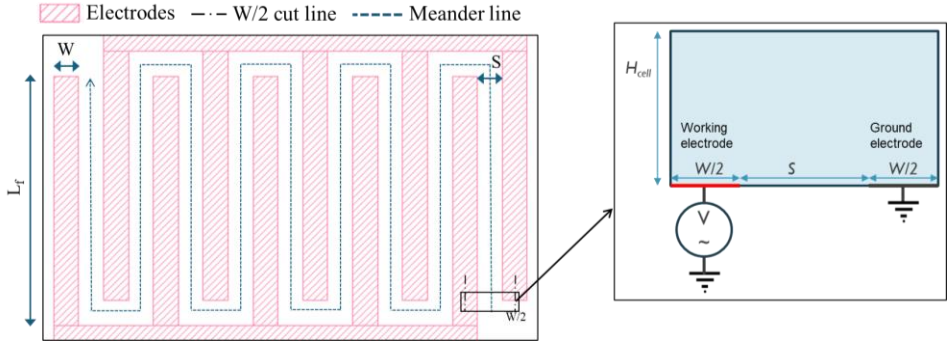


(**a**) (**b**)

**Figure 3.** (**a**) Schematic of the IDEs design of sensor for lab validation (**b**) Approximation of the IDEs design for COMSOL 2D geometry.

**Table 3.** Parameters and its values in the model.

| Symbol | Details |
|---|---|
| Electrode width, W | 600 µm |
| Spacing between electrodes, S | 600 µm |
| Length of one electrode finger, $L_f$ | 6 mm |
| Total meander length, $L_m$ | 65.1 mm |
| Electrochemical cell height, $H_{cell}$ | 600 µm |

2.2.3. Implementation

As outlined in the model definition, there are two variables to solve for: the potential in the electrolyte, $\varphi$, and the ion concentration, $c_i$. The Poisson equation, Equation (1) in Figure 2, quantifies how the electrolyte potential is affected by the space charge resulting from ion concentrations. Driven by the applied excitation voltage, ion transport takes place in the electrolyte. The ion flux consists of diffusion and migration, given by the Nernst-Planck equation, Equation (2) in Figure 2. The law of conservation of species (Equation (3) in Figure 2) allows to calculate time dependent ion concentration resulting from the fluxes.

All above equations are implemented as a time dependent study in COMSOL. Two physics modules are utilized: Electrostatics (es) and Transport of dilute species (tds). The es module is used to solve for the potential, while the tds module addresses the ion concentrations. In the es, the boundary conditions for both the working and ground electrode are implemented, as shown in Figure 2. The properties of ions, such as charge number, diffusion coefficient and the bulk ion concentrations in the electrolyte are processed in the tds module. An excitation voltage, φ(t), is applied to the working electrode with a specified amplitude and frequency. It is assumed that the electrode surface is at the point of zero charge prior to the application of this excitation voltage. However, it is acknowledged that inherent surface charge is typically present on the electrode when immersed in the electrolyte, even in the absence of an externally applied potential. Therefore, some discrepancies from the experiment are anticipated.

2.2.4. Mesh Size

At the electrode surface, where the electrode-electrolyte interface occurs, ion and voltage profiles develop during the formation of the Debye layer. This phenomenon takes place within a sub-micrometer distance from the electrode surface. To accurately capture these effects, the mesh size must be sufficiently fine. Typically, for low concentrations (e.g., 1 mM) the Debye length is ca. 1 nm [13], therefore the mesh size must be smaller than this value. A mesh size of 0.01 nm is used adjacent to the electrode surface.

2.2.5. Time Dependent Study

For time dependent study three periods of sinusoidal excitation voltage are applied to capture the rate of change in potential and ion concentration in the electrolyte. For excitation with multiple frequencies, a parametric sweep of 0.1 to 1 MHz is applied.

2.2.6. Post Processing

After the simulation run, the results for the potential drop ($\varphi$) and the electric field ($-\nabla\varphi$) in the electrolyte are processed to determine the current response and, subsequently, the impedance. The current response can be evaluated by the surface integral of the electric field normal to the surface, as given in Equation (3).

$$I_{(t)} = \oiint \epsilon_{liq} \frac{d\nabla\varphi \cdot \vec{n}}{dt} \cdot dA \quad (3)$$

Here, $A$ is the surface area of the working electrode. The impedance, Z, is expressed in the form of magnitude, |Z|, and phase shift using Bode plot representation. The magnitude of impedance is calculated, as explained in Section 2.1, for the third period of excitation. In the same cycle the phase shift is calculated from the time difference, Δt, between the peak of excitation voltage and the current response.

*2.3. Experimental*

For model validation, the EIS measurements are performed. The IDEs having 5 fingers per electrode consist of platinum electrodes on a $SiO_2$ covered silicon substrate, as shown in Figure 4a. The measurements were done using a MultiPalmSens4 using the software MultiTrace4.5 from PalmSens BV, The Netherlands. The current range could vary from 1 nA up to 10 mA, the $E_{dc}$ was set at 0.0 V and $E_{ac}$ was set at 10 mV amplitude. The EIS measurements were based on a frequency scan with a maximum frequency of 1 MHz and a minimum frequency of 0.1 Hz with 10 points per decade (71 frequencies in total).

Electrodes were fully submerged in solutions with varying NaCl concentrations in deionized water, as shown in Figure 4b. The solutions included 1, 10, and 100 mM NaCl (at room temperature), and the electrodes were rinsed with deionized water between measurements of different solutions.

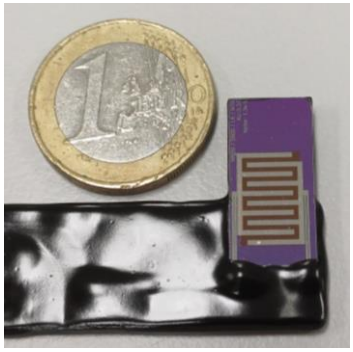

(**a**)

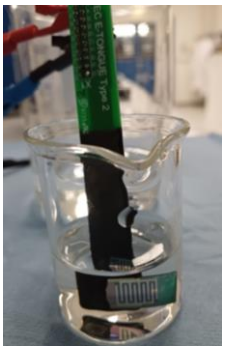

(**b**)

**Figure 4.** (**a**) IDE sensor on a Silicon substrate used for lab validation (**b**) IDE sensor in aqueous electrolyte during lab measurements.

## 3. Results

### *3.1. Voltage and Current Response Simulation*

Once the simulation has computed potentials and ion concentrations as function of time, then the current response can be calculated in the post processing using Equation (3). The ion concentration values are varied between 1 to 100 mM. The plots of the first half-period of the excitation voltage (10 mV amplitude sinusoidal), voltage drop at the electrode and current response at 0.1 Hz for 1 and 100 mM NaCl concentrations are shown in Figure 5. The phase shift between voltage and current is 90° for both the concentrations, which means at low frequency the Debye layer is formed to contribute to the electric double layer capacitance. Moreover, the voltage at the electrode is lower than the excitation voltage, i.e., 9.75 mV (Figure 5a) and 8.29 mV (Figure 5b) amplitude for 1 mM and 100 mM concentrations, respectively. This is caused by the voltage drop of the Stern layer and the sheet resistance.

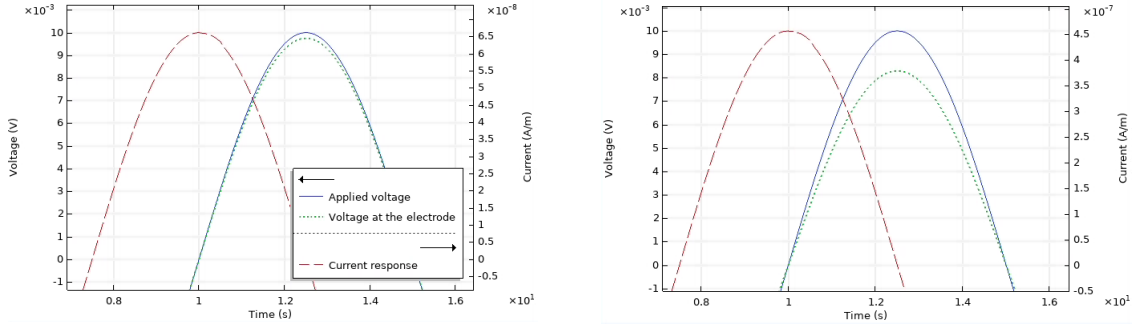


(**a**) (**b**)

**Figure 5.** Plot of first half-cycle of the applied voltage, voltage drop at the electrode surface and the current response at 0.1 Hz for (**a**) 1 mM and (**b**) 100 mM NaCl concentration.

The time dependent analysis is computed for three periods of voltage excitation to capture the time-dependent behavior of the system at different frequencies (0.1 Hz to 1 MHz). The voltage and current response over time for various frequencies at 1 mM NaCl concentration is shown in Figure 6. These frequencies are chosen to show interesting region, i.e., 0.1 Hz (lowest frequency), 100 Hz (near the cutoff frequency where the phase shift is 45°), 2.15 kHz (frequency of the lowest phase shift) and 1 MHz (highest frequency).

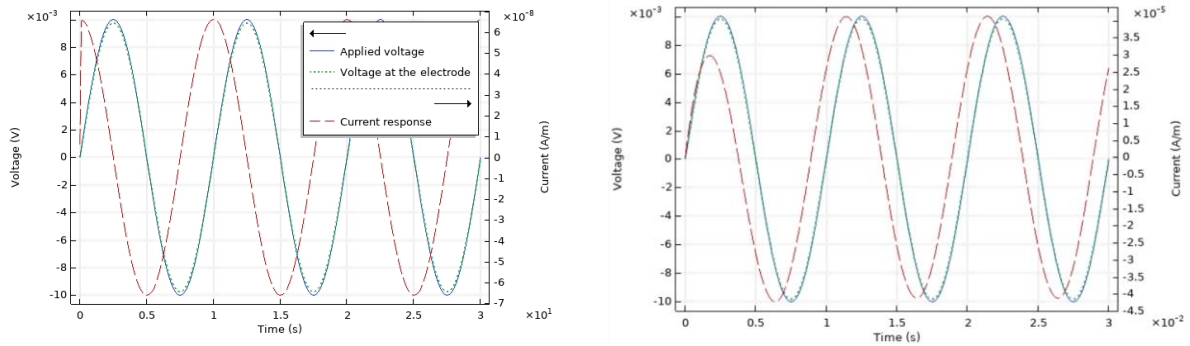


(**a**) (**b**)

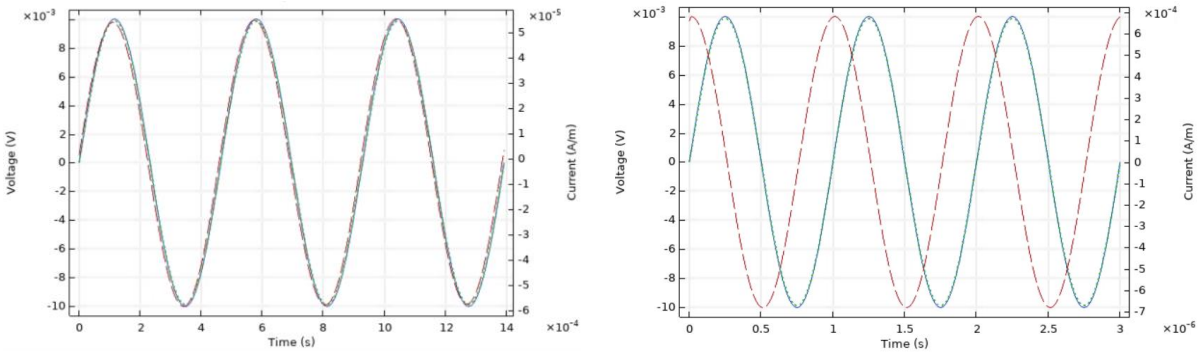


(**c**) (**d**)

**Figure 6.** Plots of applied voltage, voltage drop at the electrode surface and the current response of 1 mM NaCl electrolyte at (**a**) 0.1 Hz, (**b**) 100 Hz, (**c**) 2.15 kHz and (**d**) 1 MHz.

Similarly, the voltage and current response for 100 mM concentration are also computed. The plot for various frequencies of interest, i.e., 0.1 Hz (lowest frequency), 464 Hz (near the cutoff frequency), 10 kHz (frequency of the lowest phase shift) and 1 MHz (highest frequency), are shown in Figure 7.

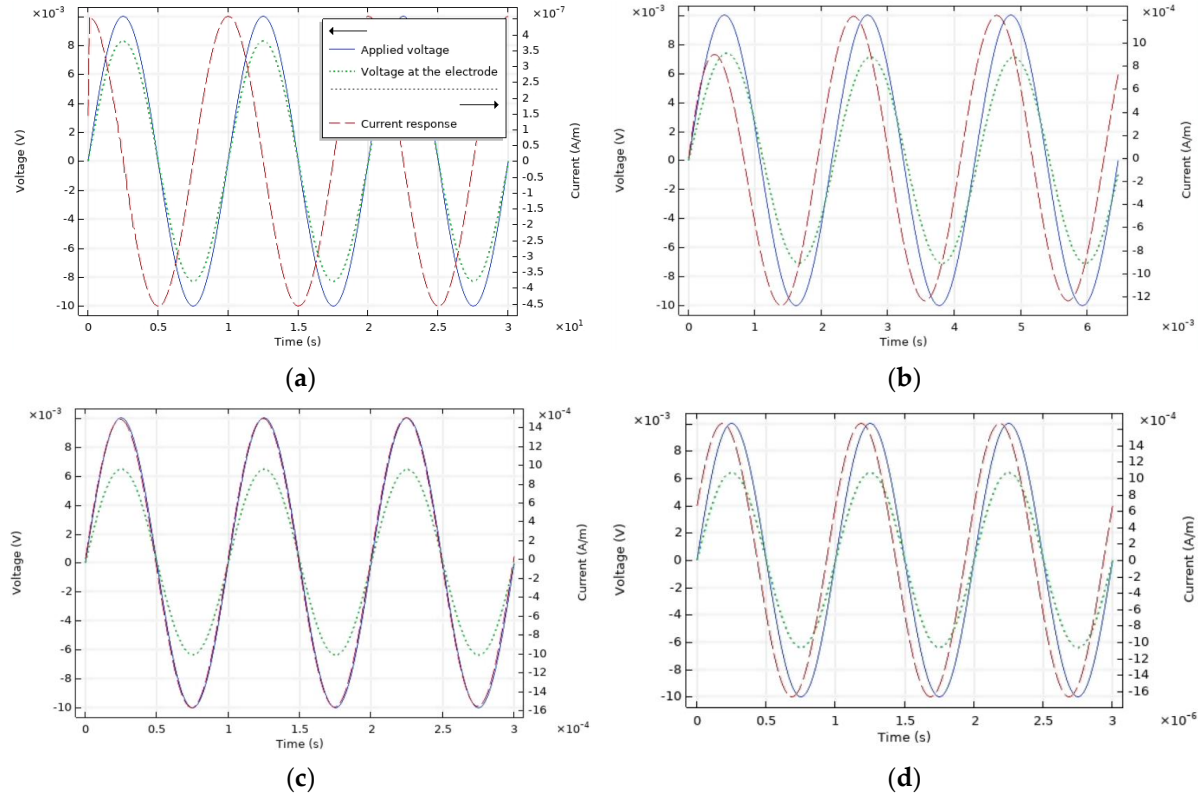


(**a**) (**b**)

(**c**) (**d**)

**Figure 7.** Plots of applied voltage, voltage drop at the electrode surface and the current response of 100 mM NaCl electrolyte at (**a**) 0.1 Hz, (**b**) 464 Hz, (**c**) 10 kHz and (**d**) 1 MHz.

### *3.2. EIS Results*

From the current response and excitation voltage simulation, the impedance response—the magnitude of impedance and the phase shift—is evaluated, as described in the post-processing Section 2.2.6. The impedance plots for the frequency sweep between 0.1 Hz and 1 MHz at various concentrations are shown in Figure 8 as a Bode plot. For comparison, the experimental values of impedance, labeled as 'exp', are also plotted in this figure. The simulation results are labeled as 'sim'. The magnitude of impedance and

the phase shift for 1 mM, 10 mM, and 100 mM NaCl concentrations are compared in Figure 8a and Figure 8b, respectively.

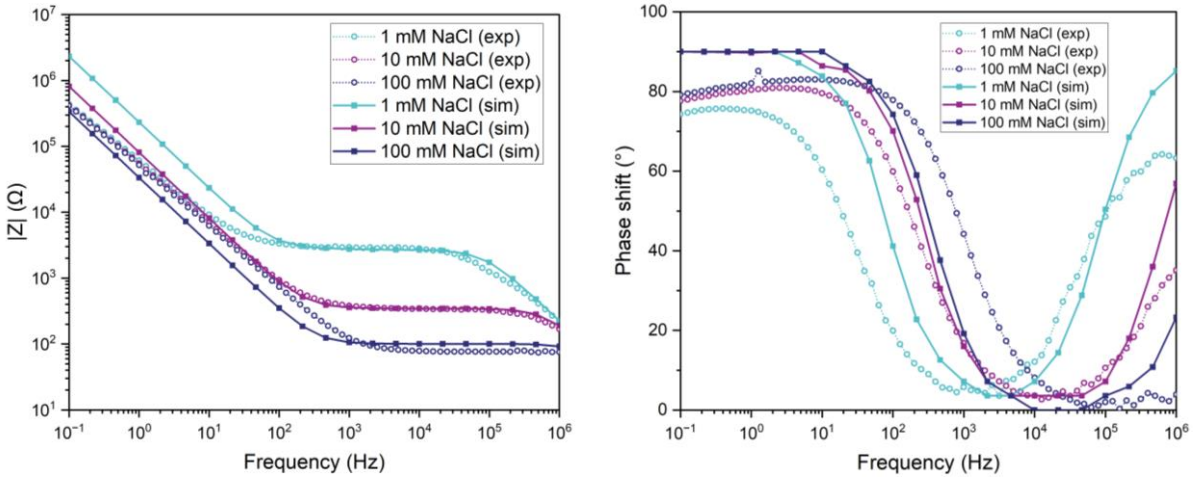


(**a**) (**b**)

**Figure 8.** Bode plot of impedance over excitation frequency range at 1, 10 and 100 mM NaCl solution from lab experiment and simulations (**a**) Magnitude of impedance, |Z|, vs. excitation frequency (**b**) Phase shift vs. excitation frequency.

## 4. Discussion

In Figure 5, the half-period of the voltage and current plot shows the potential at the electrode surface for 0.1 Hz for 1 and 100 mM ion concentration. The voltage at the electrode shows lower values as compared to the external excitation voltage. This voltage-drop is contributed by the Stern layer drop and the sheet resistance of the electrode. At lower excitation frequencies, for example at 0.1 Hz, the stern layer dominates, i.e., 0.25 mV and 1.71 mV for 1 and 100 mM, respectively, are due to Stern layer, whereas the voltage-drop due to the sheet resistances are 0.3 μV and 1.25 μV, respectively. At high frequencies, greater than the cutoff frequency, the voltage-drop due to sheet resistance become significant. At 1 MHz, the voltage-drops from the sheet resistance for 1 and 100 mM are 0.14 mV and 3.6 mV, respectively, and the Stern layer voltage-drops are negligible (ca. 1 μV).

At lower frequencies, such as 0.1 Hz, there is sufficient time for ions to transport and form the EDLC resulting in a 90° phase shift, as shown in Figures 6a and 7a. With the increase in the excitation frequency, the EDLC diminishes and the phase shift between the voltage and the current response reduces. Around the cutoff frequency the phase shift is ca. 45°, as shown in Figures 6b and 7b. Consequently, the electric field and voltage drop over the Stern layers becomes negligible with the further increase in the excitation frequency and the phase shift approaches to zero degrees, as shown in Figures 6c and 7c. The current over the sheet resistance is highest at higher frequencies, resulting in a higher voltage-drop over the sheet resistance. At these frequencies the magnitude of impedance is resistive and comprises of the electrolyte bulk resistance and the sheet resistance of the electrode. For 1 mM concentration, the voltage at the working electrode is close to the excitation voltage, however, for 100 mM the amplitude of the potential at the working electrode decreases to 6.4 mV. The higher drop at 100 mM is because the electrolyte resistance becomes comparable to the sheet resistance, causing a higher voltage-drop due to the sheet resistance (3.6 mV). The total system resistance at 10 kHz is equal to $R_s + 2R_{el}$ (resistors in series). The total impedance is known at this frequency (see, Figure 8a for 100 mM concentration) and the individual resistance can be estimated from the voltage divider theory [14]. At 100 mM concentration and 10 kHz excitation frequency, the sheet resistance value is estimated to be ca. 35 Ω, whereas the electrolyte resistance value is ca. 30 Ω. This is another practical aspect to be considered when determining the electrolyte

resistance for higher concentrations through EIS measurements. Furthermore, at much higher frequencies, i.e., 1 MHz, the parasitic capacitance effect from the $SiO_2$ layer on silicon substrate comes into effect, as shown in Figures 6d and 7d, where the phase shift is 23.3° and ca. 85° for 1 and 100 mM, respectively. Therefore, this limitation of the parasitic capacitance from $SiO_2$ needs to be considered when designing an EIS-based sensor on a silicon substrate.

Another interesting observation is the time dependent behavior of the current response. In Figures 6b and 7b, the current response shows lower peak values in the first period as compared to the last period. The current needs some time to stabilize from a transient into a periodic response. For EIS measurement it is important to know how many periods are required to reach a periodic current response before estimating the impedance. This is an important input for experiments, since in the experimental setup, a certain number of periods of excitation is applied before estimating the impedance.

The comparison of the |Z| and phase shift for the simulated and experimental values for 1, 10 and 100 mM shows the same characteristic features, albeit not exactly matching. For 1 mM ion concentration, the plateau of the lower phase shift (after the cutoff frequency) starts after 1 kHz for simulation as well as for experiments. The |Z| value at this plateau is 2.7 k Ω, which is purely resistive, as evident from the phase shift which is close to zero degrees. At even higher frequencies (above 100 kHz), the parasitic effect of $SiO_2$ starts appearing in the impedance plot with the increase in the phase shift, (up to ca. 85° at 1 MHz for 1 mM concentration). For higher concentrations, i.e., 10 and 100 mM, the effect of parasitic capacitance is shifted to higher frequency as until 1 MHz the phase is increased to 56.88° and 23.3°, respectively. This is because the lower electrolyte resistance values at high ion concentrations, decreases the RC time in combination with the parasitic capacitance.

In Figure 8a, the |Z| values at the low-phase-shift plateau (electrolyte resistance plateau) for both the simulation and the experiment decrease with the increase in ion concentration. But this decreasing step is not proportional, especially for higher concentrations. From 1 mM to 10 mM the plateau reduced from ca. 2.7 k Ω to 0.34 k Ω, which is ca. 8 times reduction when the concentration is increased 10 time. From 10 mM to 100 mM, the |Z| reduced from 0.34 k Ω to 0.1 k Ω, which is a reduction of 3.4 time. This means at higher concentrations, the |Z| plateau does not correspond proportional to the ion concentration and shows a saturation at higher concentrations. This saturation is due to the sheet resistances. In this case once the electrolyte resistance, $R_s$, goes below 100 Ω, the contribution of sheet resistance (ca. 35 Ω) becomes significant. Therefore, when designing an EIS sensor for higher concentration, it is important to consider the limitation due to the sheet resistance.

When comparing the |Z| plot, Figure 8a, of simulation and experiment at low frequencies (<100 Hz), the simulation data shows similar slopes, ca.−1/decade in the log scale for all the concentrations. The experiments converge into a single curve at low frequencies but exhibit an offset when compared to the simulations. There is an offset in |Z| values between these slopes which is proportional to the electrolyte concentration, i.e., at 0.1 Hz the |Z| increase 2.4 times when going from 100 mM to 10 mM and 2.8 times increase from 10 mM to 100 mM. This means for simulation at low frequencies the EDL capacitance is dominated by the Debye layer, which is concentration dependent. This is as expected since in this model, the Stern layer is modeled as a fixed thickness which is independent of ion concentration and the Debye layer becomes the dominating factor at these frequencies. Interestingly, the |Z| plot for experimental data shows closer slope values to the simulation, i.e., ca. −0.85/decade in log scale, however there is no offset between values for different concentrations. The |Z| values for all concentration converged to similar values around 420 kΩ. This could be due to any Faradaic reaction or adsorption/desorption kinetics at the electrode surface which are not considered in the COMSOL model. Similarly, in the phase shift plot for simulation results, Figure 8b, the phase shift for all the ion concentration at low frequencies (<100) goes to 90° showing the behavior of a capacitor.

However, the experimental phase shifts deviate from pure capacitive behavior and show lower values, i.e., at 0.1 Hz around 80°, and shows a trend of decrease phase shift when reducing frequency. This suggests that there can be an additional component missing in the model at low frequencies. This will be further addressed in future work.

## 5. Conclusions

A time-dependent electrochemical impedance spectroscopy (EIS) model using finite element analysis in COMSOL Multiphysics has been developed. This model addresses the transport of ions in an electrolyte under an external excitation voltage applied at the electrode. The core of the model relies on two primary domain equations: the Poisson equation and the Nernst-Planck equation. The interdigitated electrode is approximated as a 2D geometry in COMSOL, represented as two parallel planar electrodes—working and ground. A sinusoidal excitation voltage is applied to the working electrode, and the resulting current response is evaluated.

Key boundary conditions include the Stern layer drop, modeled with a fixed Stern layer thickness of 0.5 nm, and the voltage drop due to sheet resistance. The time-dependent study involves three periods of excitation to capture the dynamic behavior of the system. Simulations were conducted for three different ion concentrations—1 mM, 10 mM, and 100 mM NaCl. These simulations were validated against experimental data for the same concentrations.

The analysis reveals that at a concentration of 1 mM, the Stern layer voltage drop is significant at lower frequencies (e.g., 0.25 mV at 0.1 Hz) but diminishes as frequency increases beyond the cutoff. For higher concentrations, the voltage-drop at the electrode results from both the Stern layer and sheet resistance. Even at high frequencies, where the Stern layer effect reduces, the voltage drop remains considerable (approximately 3.5 mV, or 35% of the excitation voltage amplitude). This highlights the importance of accounting for sheet resistance, especially at lower concentrations, to ensure that the electrode design achieves higher electrolyte resistance relative to the sheet resistance and help setting right excitation voltage during experiments.

The current response from the time dependent analysis in the model shows variation over time in some cases, the current response needs some time for stabilizing to a fully periodic signal. In this study three periods of excitations were enough to stabilize the current response. This is an important insight that a time-dependent model can provide. The practical implication is that the EIS can be simulated before experiment on such a time-dependent model to determine how many cycles of excitation are needed before estimating the impedance from the voltage-current response.

Comparing experimental data with simulation results, the EIS plots for magnitude |Z| and phase shift exhibit close agreement, particularly at higher frequencies (>cutoff frequency). At frequencies such as 1 MHz, parasitic effects from the SiO2 layer on the silicon substrate become significant, with these effects shifting to lower frequencies as ion concentration decreases. Therefore, for silicon-based sensors, considering the parasitic capacitance of SiO2 is crucial, especially for lower ion concentrations (below 1 mM).

At low frequencies, the experimental |Z| data converge to a similar value across concentrations, though the simulation shows a frequency-dependent offset in |Z| values. The phase shift in the experimental data is consistently lower than in the simulations, suggesting that additional elements may need to be incorporated into the model for accurate representation at lower frequencies. This aspect will be explored in future work to extend the model's accuracy.

While the model simplifies certain aspects of the system, it provides significant insights into the physicochemical processes during EIS excitation. It proves valuable for designing EIS-based sensors and optimizing experimental parameters, demonstrating its utility despite its approximations. Moreover, for biosensing application when a bio-sensitive layer is added, hence changing the adsorption/desorption dynamics, such a time dependent model can be valuable to determine the steady state.

**Author Contributions:** Conceptualization, Y.A., J.F.M.O., M.A.G.Z. and A.R.M.V.; methodology, Y.A. and L.v.S.; software, Y.A.; validation, L.v.S.; investigation, Y.A., J.F.M.O. and A.V; writing—original draft preparation, Y.A.; writing—review and editing, Y.A., L.v.S., J.F.M.O., M.A.G.Z. and A.R.M.V.; visualization, X.X.; supervision, J.F.M.O. and A.R.M.V.; project administration, J.F.M.O. All authors have read and agreed to the published version of the manuscript.

**Funding:** This project is made possible by a contribution from the National Growth Fund program NXTGEN HIGHTECH.

**Institutional Review Board Statement:**

**Informed Consent Statement:**

**Data Availability Statement:** The data presented in this study are available on request from the corresponding author.

**Conflicts of Interest:** The authors declare no conflict of interest.

## References

1. Mostafa, I.; Brederlow, R. Trends, Challenges, and Recent Advances in Electrochemical Impedance Spectroscopy. *IEEE Sens. Lett.* **2022**, *6*, 5500604.
2. Preethichandra, D.M.G.; Sonar, P. Electrochemical Impedance Spectroscopy and Its Applications in Sensor Development and Measuring Battery Performance. *IEEE Sens. J.* **2021**, *22*, 10152–10162.
3. Pourmir, A.R.; Bahrmand, A.R.; Ettefagh Far, S.H.; Hadizadeh Tasbiti, A.R.; Yari, S. Rapid Diagnosis of Mycobacterium Tuberculosis with Electrical Impedance Spectroscopy in Suspensions Using Interdigitated Microelectrode. *J. Anal. Chem.* **2016**, *71*, 676–684.
4. Lazanas, A.C.; Prodromidis, M.I. Electrochemical Impedance Spectroscopy—A Tutorial. *ACS Meas. Sci. Au* **2023**, *3*, 162–193.
5. Brom-Verheijden, G.J.A.M.; Goedbloed, M.H.; Zevenbergen, M.A.G. A Microfabricated 4-Electrode Conductivity Sensor with Enhanced Range. *Proceedings* **2018**, *2*, 797.
6. Abbas, Y.; Jaspers, M.; Moalla, R.; van Nieuwstadt, J.; Zevenbergen, M.A.G. Electrical Conductivity Sensor for Plant Substrates. *Proceedings* **2024**, *97*, 135.
7. Vivier, V.; Orazem, M.E. Impedance Analysis of Electrochemical Systems. *Chem. Rev.* **2022**, *122*, 11131–11168.
8. Saghafi, M.; Chinnathambi, S.; Lemay, S.G. High-Frequency Phenomena and Electrochemical Impedance Spectroscopy at Nanoelectrodes. *Curr. Opin. Colloid Interface Sci.* **2023**, *63*, 101654.
9. R-Smith, N.A.-Z.; Leitner, M.; Alic, I.; Toth, D.; Kasper, M.; Romio, M.; Surace, Y.; Jahn, M.; Kienberger, F.; Ebner, A. Assessment of Lithium Ion Battery Ageing by Combined Impedance Spectroscopy, Functional Microscopy and Finite Element Modelling. *J. Power Sources* **2021**, *512*, 230459.
10. Häffelin, A.; Joos, J.; Ender, M.; Weber, A.; Ivers-Tiffée, E. Time-Dependent 3D Impedance Model of Mixed-Conducting Solid Oxide Fuel Cell Cathodes. *J. Electrochem. Soc.* **2013**, *160*, F867.
11. Guggenheim, E.A. The Diffusion Coefficient of Sodium Chloride. *Trans. Faraday Soc.* **1954**, *50*, 1048–1051.
12. Brown, M.A.; Goel, A.; Abbas, Z. Effect of Electrolyte Concentration on the Stern Layer Thickness at a Charged Interface. *Angew. Chem.* **2016**, *128*, 3854–3858.
13. Dickinson, E.J.F.; Limon-Petersen, J.G.; Compton, R.G. The Electroneutrality Approximation in Electrochemistry. *J. Solid State Electrochem.* **2011**, *15*, 1335–1345.
14. Li, B.; He, Y.; Wang, L.; Cao, M.; Fu, Z.; Zhang, H. Calibration Method of a Wideband AC Resistance Voltage Divider Based on an Equivalent Model. *Sensors* **2023**, *23*, 7181.